Reflection and attachment of spirals at obstacles for the Fitzhugh-Nagumo and Beeler-Reuter models

Daniel Olmos*

Departamento de Matemáticas, Universidad de Sonora, Boulevard Luis Encinas y Rosales, Colonia Centro, Hermosillo, Sonora 83000, México

(Received 16 December 2008; revised manuscript received 18 March 2010; published 30 April 2010)

In this paper, the Fitzhugh-Nagumo (FHN) equations and a modified FHN (MFHN) are considered. For the modified version, the recovery variable v has three different time scales. By considering different parameters in the local dynamics of the MFHN equations, it is observed that the phenomenon of reflection and annihilation at an impermeable boundary is observed just as in the Beeler-Reuter model. The interaction of spirals obtained with the FHN, MFHN, and Beeler-Reuter model, and an obstacle is also considered. The phenomenon of reflection of the spiral wave at a boundary changes when the boundary becomes an obstacle. Four properties for attachment of a spiral wave to an obstacle are presented in this work.

DOI: 10.1103/PhysRevE.81.041924 PACS number(s): 87.10.−e, 87.19.Hh, 82.40.Ck, 87.64.Aa

I. INTRODUCTION

The study of spiral waves in excitable media modeled with reaction diffusion equations [1–6] is an important research area [1,7,8]. Spiral waves appear in chemical reactions, in models of the electrical activity of the heart as well as the spreading of depression waves in the chicken retina [1–6]. The study of the interaction between spiral waves and impermeable obstacles [9–14] is a significant problem in cardiac physiology. When a spiral wave attaches to an obstacle, the irregular polymorphic electrical activity ends and a periodic monomorphic activity emerges [10,14,15]. This transition is clinically important because as it has been shown fibrillationlike activity changes to a tachycardia regime [15]. Therefore, the understanding of the interaction of a spiral wave in the meandering regime with an obstacle is an important problem.

The interaction between spiral waves and obstacles has been experimentally and computationally studied by different researchers [9,10,12,13]. Shajahan *et al.* [12] used the Luo-Rudy and Panfilov models to study the transition of spiral turbulence to a simple rotating spiral wave due to the presence of an obstacle; from their experimental work on the interaction of a spiral wave with obstacles, Ikeda *et al.* [10] concluded that a spiral wave always attaches to an obstacle of minimal size; Panfilov and Keener studied the interaction of successive wave fronts interacting with an obstacle and showed that this could be a mechanism for spiral wave initiation [11]; Comtois and Vinet [13] studied the partial detachment of a spiral wave at an obstacle in a two-dimensional annulus. Azene *et al.* [9] carried out a computational study of the attachment and detachment of wave fronts to obstacles based on the Luo-Rudy model. Olmos and Shizgal [16] carried out a study of the reflection and annihilation of spiral waves at a domain boundary using the Beeler-Reuter (BR) equations, a model for ventricular cardiac cells. They considered spiral waves in the meandering regime, particularly when the petals lie on a straight line, that is, the R_∞ regime. The aim was to understand the interaction of spiral waves in a meandering regime with a domain boundary by approximating the meandering regime with the R_∞ regime near to the boundary. The spiral-wave boundary interaction not in the R_∞ regime is complex [16]. Even though the domain boundary can be seen as a large obstacle, the interaction spiral-wave boundary is different than interaction spiral-wave obstacle as will be shown in this work.

The interaction between a meandering spiral wave and an obstacle has not been previously considered. Such interactions can be very complex [16,17] and the determination of the conditions for which a meandering spiral wave will attach to an obstacle is an important endeavor. Shajahan *et al.* [12] considered the effect of the size and the location of an obstacle on the transition of spiral turbulence into rotating spirals. However, the actual mechanism by which this transition was not considered.

In order to reduce the computational cost in the simulations and to preserve properties of complex models, modifications of the Fitzhugh-Nagumo (FHN) equations or simplifications of more complex models have been considered [11,12,17–21]. Among these models are the Panfilov and Keener model [22]; the Bernus *et al.* model [18] which is a simplification of the Priebe-Beuckelmann model [19]; or the Ten-Tusscher and Panfilov model [20] which is a simplification of the model presented by Ten-Tusscher and Panfilov [21]. The Bueno-Orovio-Cherry-Fenton minimal model [23] is designed to mimic the behavior of complex models with a minimum number of variables.

In [16], the phenomenon of annihilation of spiral waves at a boundary studied with the BR dynamics in the R_∞ regime was not replicated with the FHN model [16]. In this paper, we employ a modified version of the FHN equations in order to obtain annihilation and reflection of a spiral wave at a boundary in the R_∞ regime analogous to what was observed in [16]. We explain why the modified FHN model, a variant of the Panfilov and Keener model [22], shows both types of behaviors. We show that the size and geometry of the obstacle, excitability of the medium, ratio of the area to be excited and length of the front near the trajectory of the tip, control the attachment of a spiral wave to the obstacle. The

*olmos@gauss.mat.uson.mx

results obtained in this study can be applied to more general models because the ideas are based on arguments of excitability and recovery properties of the medium. These results can be also used to determine, for a given conductivity of the medium, the size and geometry of the obstacle that maximizes the attachment possibility. In Sec. II, the model equations used in the numerical experiments are presented. In Sec. III, a description of the numerical method used is provided. Numerical studies and results are given in Sec. IV. In Sec. IV A the dynamics of a spiral wave with the modified FHN equations are presented and a study of the interaction of a spiral wave with a boundary is also shown. In Secs. IV B and IV C, the interaction between a spiral wave and an obstacle with the FHN as well as the modified FHN equations is considered. In Sec. IV B it is also shown for FHN the difference of considering the interaction of a spiral and an obstacle or a boundary. We also discuss the conditions that allow the attachment of a meandering spiral wave to an obstacle. Finally, a summary of the results and conclusions is presented in Sec. V.

II. MODEL EQUATIONS

We consider a reaction-diffusion model with local dynamics defined by a modified version of the Barkley model [24], that is,

$$\frac{\partial u}{\partial t} = D\nabla^2 u + \frac{1}{\epsilon}u(1-u)(u-u_{th}),$$

$$\frac{\partial v}{\partial t} = \delta(u,v)(u-v), \tag{1}$$

where $D=1$ is the diffusion coefficient, $u_{th}=(v+b)/a$, a, b, and ϵ are dimensionless parameters and δ is a function of u and v. When δ is equal 1, we have the traditional FHN equation. For the modified FHN (MFHN) model, δ varies with u and v. Equation (1) is similar to the one studied by Panfilov and Keener [22,25], in the sense of that the recovery variable v has different time scales. The value of δ is taken as δ_1 if $u<0.2$ and $v>0.2$; $\delta=\delta_2$ if $u<0.2$ and $v\in[0.05,0.2]$ and $\delta=\delta_3$ otherwise. The choice of δ in these regions does not modify the speed of the wave compared to the original FHN equation provided that the value of v at the front of the wave is less than 0.05. In this work, $\delta_2=5$ and $\delta_3=1$, and we focus on the effect of δ_1 on the local dynamics of v. The effect of the different values of δ_1 on the dynamics of v is shown in Fig. 1, where the profiles of u and v for a propagating pulse in one dimension are shown for a fixed value of t. In the figure, the profiles with the FHN model, i.e., Equation (1) with $\delta=1$ and the MFHN with $\delta_1=0.3$, $\delta_1=0.6$ are compared. The profiles of u for the three cases are indistinguishable from each other and are shown by the gray curve (Fig. 1). The profiles for v are shown for the FHN model (solid thin curve) and MFHN with $\delta_1=0.6$ (dashed) and $\delta_1=0.3$ (bold). In Eq. (1), the larger is δ_1, the shorter is the refractory time of the medium. The inactivation process, controlled by δ_3, occurs on a faster time scale than the reactivation process, controlled by δ_1 and δ_2 (Fig. 1). Therefore, the

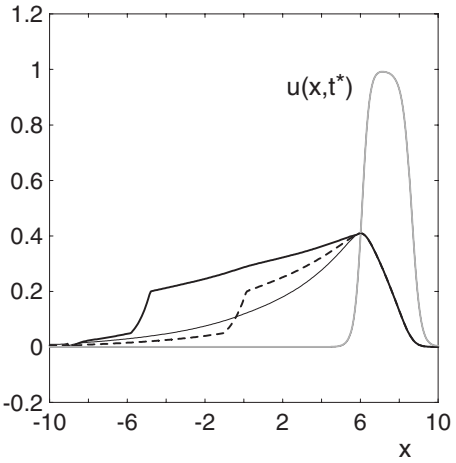

FIG. 1. Solutions $u(x,t^*)$, $v(x,t^*)$ at a time t^* for the FHN and MFHN equations in one dimension. $u(x,t^*)$ is the same for all the cases and is shown in gray. $v(x,t^*)$ for the FHN (thin solid) and for MFHN with $\delta_1=0.6$ (dashed) and $\delta_1=0.3$ (bold).

MFHN model simulates the effects of the variables h and j for inactivation and reactivation of the sodium current in the BR model [26].

In this paper, we focus our studies on spiral waves in the R_∞ case, i.e., when the petals of the meandering tip trajectory lie on a straight line as in [16]. The R_∞ case is of great importance because it helps to understand the interaction of a spiral wave in the meandering regime and an unexcitable object. For the FHN equations, the values $a=0.63$, $b=0.05$, and $\epsilon=0.02$ give the R_∞ case. For the MFHN model, $\epsilon=0.02$ and $b=0.01$ implies that for $\delta_1=0.6$ and $\delta_1=0.65$ the values of $a=0.5085$ and $a=0.52$, respectively, give tip trajectories in the R_∞ regime.

III. NUMERICAL METHODS

The solution of Eq. (1) is obtained with the pseudospectral methods based on Chebyshev polynomials as described in [27]. The domain considered is the square $\Omega=[-10,10]\times[-10,10]$. In each dimension, the domain was divided into N_i overlapped subdomains of the same length. Each subdomain has N_{ch} Chebyshev-Gauss-Lobatto collocation points [27]. The subdomains have in common two points giving a total of $N=(N_{ch}-2)N_s+2$ points in each dimension [27]. The resulting equations were integrated in time using a second order Runge-Kutta scheme. In this work, $N_i=40$ and $N_{ch}=10$ giving a total of 322 points in each dimension and the integration time step $\Delta t=0.0001$ is used.

In order to model an obstacle, no flux boundary conditions are imposed, as done in [11,12]. In Fig. 2, we illustrate the model of an obstacle (in black) in two dimensions and the application of boundary conditions. The numerical methods used require that the obstacle has a rectangular shape and boundary coinciding with an extremum of a subdomain as shown in Fig. 2.

Different obstacle or domain geometries can be modeled with other methods such as the one proposed by Bueno-Orovio *et al.* [28]. However, one of the advantages of the

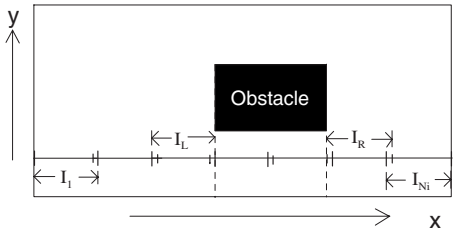

FIG. 2. Illustration of the modeling of an obstacle with no flux at the boundary of the obstacle. In the x direction it is shown that the obstacle starts at the end of the interval I_L and ends at the beginning of the subinterval I_R. The same rule follows in the y direction.

method presented in this work is that the numerical solution gives a very good approximation to the converged solution with only 322 points in each dimension as discussed in [27]. The accuracy of the numerical solution is particularly important near the obstacle due to the spiral wave-obstacle interaction [16]. The method in [28] might not be suitable to study such interaction due to the presence of a neighborhood of width ξ at the boundary of the obstacle, which can be a significant source of error for the solution near the obstacle.

Tip trajectories with incident angle θ_i with respect to a boundary were considered as in [16]. In order to generate a spiral wave with incident angle θ_i for the FHN and MFHN models, an initial solitary pulse is generated with the initial condition of the form

$$u(x,y) = \{1 + \exp[k(|y + \alpha y| - r_1)]\}^{-2} - \{1 + \exp[k(|y + \alpha y| - r_2)]\}^{-2}, \quad (2)$$

$v(x,y)=0$, and where u is taken as zero for $\alpha x > -y$. After some integration time, a free end on this solitary pulse is induced in order to generate a spiral wave. At the time t_s and for 0.1 units of time, the solution is redefined in the region $\alpha y < x - x_0$ as $u=0$ and $v=0.25$. Initially, in Eq. (2) α was taken as zero, $r_1=9.8$, $r_2=9$, $t_s=1.2$, $k=4$, and $x_0=0$, for the case of $\delta_1=0.6$. With these values, a spiral wave in the R_∞ regime was generated such that the incident angle was $\theta_i=61.5°$. For a different incident angle θ_i, the value of α in Eq. (2) was taken as $\alpha=\tan((\theta_i-61.5)\pi/180)$ and the values of r_1, r_2, t_s, and x_0 were taken such that the spiral wave was inside the domain and initial boundary effects were avoided, analogous to the procedure used for the BR model [16].

The tip trajectories for the FHN and the MFHN models were found with the intersection of level curves with the method described by Barkley [24], whereas for the Beeler-Reuter model the point with zero normal velocity as discussed by Fenton *et al.* [1].

IV. NUMERICAL RESULTS

In this section, we present results obtained with the FHN, the MFHN, and the BR equations. We consider first the phenomenon of reflection and annihilation of a spiral wave at a boundary with the MFHN model and then proceed to study the interaction between a spiral wave obtained with the three models and an obstacle.

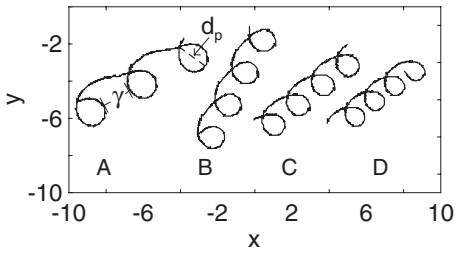

FIG. 3. Tip trajectories in the R_∞ regime obtained with the MFHN equations for different values of δ_1: (A) 0.45, (B) 0.6, (C) 0.65, and (D) 0.75. γ is the distance between petals and d_p is the diameter of a petal given by the largest distance between points lying on the petal.

A. Reflection and annihilation with the MFHN model

We first consider the MFHN equations with different values of δ_1 and study the effects on the spatial dynamics. Figures 3(A)–3(D) show different tip trajectories in the R_∞ regime obtained with different values of $\delta_1=0.45$, 0.6, 0.65, and 0.75, respectively. The smaller the value of δ_1, the larger is the recovery time of the medium, and in Fig. 3 a larger recovery time is associated with larger arcs. However, a better measure of the effect of δ_1 on the spatial dynamics is given by $\eta=\gamma/d_p$, where γ is the distance between two petals (Fig. 3) and d_p is the diameter of a petal, which is given by the largest distance between points lying on a petal. The quantity η is a measure of the relative size between the petals and the arcs. In Figs. 3(A)–3(D), the values of γ are 1.64, 0.75, 0.59, and 0.37, and the values of d_p are 1.75, 1.43, 1.38, and 1.2, respectively. This implies that η is equal to 0.94, 0.52, 0.43, and 0.31 for the trajectories A–D in Fig. 3, respectively. A larger value of η implies that there is a higher probability of hitting a boundary with an arc, and therefore increasing the probability of annihilation of the spiral wave at the boundary [16]. An increase in η means that γ increased faster than d_p and where, by using scaling arguments, it is equivalent to consider a fixed value of d_p and an increase in γ. Physically, this corresponds to have a longer recovery period (larger γ) for a fixed d_p.

The physiological parameters for controlling the value of η are model dependent and are not the primary interest in this work. However, the value of η is independent of the model considered. In [16], the values of γ and d_p for the BR model, for which annihilation was observed, are 5.0 and 4.51 units of length respectively, giving $\eta=1.10$. For the FHN equations [16], where no annihilation was observed, $\gamma=0$ and $d_p=1.64$ units, gives $\eta=0$. Therefore, a value $\eta=\eta^*$ exists for the R_∞ regime, such that below η^* no annihilation is present and above η^* annihilation is possible. The different scenarios by which annihilation and reflection are observed for a fixed incident angle was discussed in detail in [16] with the BR model.

Therefore, we study the interaction between a spiral wave and the boundary of a square domain as in [16]. With the FHN model, the phenomenon of annihilation of a spiral wave at a boundary was not observed [16]. Therefore, we considered the MFHN with $\delta_1=0.6$ and $\delta_1=0.65$. For each value of δ_1 we followed the same procedure as in [16] where

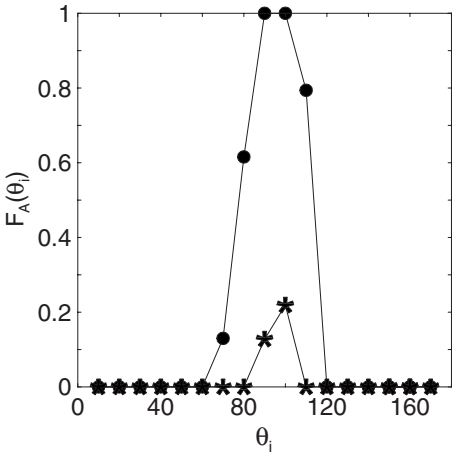

FIG. 4. Fraction of the trajectories that were absorbed by the boundary (P_A) as a function of the incidence angle θ_i for the MFHN equations with $\delta_1=0.6$ (●) and $\delta_1=0.65$ (asterisks). The angle θ_i is in degrees.

we calculated the fraction $F_A(\theta_i)$ of spiral waves that annihilated at the boundary for a fixed incident angle θ_i. For each angle θ_i we followed the same procedure as in [16] in order to obtain all the possible interactions of the spiral wave with the boundary. In order to obtain the fraction of spirals that disappeared at the boundary, we considered from 43 to 73 runs for each angle.

The results for the MFHN with $\delta_1=0.6$ (●) and $\delta_1=0.65$ (asterisks) are shown in Fig. 4 where $F_A(\theta_i)$ is plotted versus θ_i. From Fig. 4, it is shown that annihilation of the spiral wave is observed when $\delta_1=0.6$ and $\theta_i \in [70,110]$, whereas for $\delta_1=0.65$ annihilation is observed for $\theta_i \in [80,90]$. The increase in the probability of the annihilation of a spiral wave at a boundary is related to the increase in the value of η. This corresponds to an increase in the time where the medium is in refractory state. This is consistent with the results in Fig. 3, where a larger value of η increases the probability of the annihilation of a spiral wave at a boundary.

For the MFHN model, it is possible to control the values of γ and d_p and remain in the R_∞ regime. These parameters are not that easily controlled in the BR or more complex models. This advantage of the MFHN model permits the study of interaction between a spiral wave and a boundary while in the R_∞ regime for different values of γ and d_p.

B. Interaction of spirals with obstacles for the FHN model

The effect of annihilation and reflection of a spiral wave at a domain boundary can be considered when the boundary becomes an obstacle. In cardiac physiology, a vein or ischemic tissue can be considered as obstacles [12]. When considering obstacles, the effect of reflection is the same for a boundary and for the obstacle. However, the effect of annihilation at a boundary becomes attachment of the spiral wave to the obstacle.

In this section we consider the interaction of a spiral wave obtained with the FHN equations and an obstacle. In both,

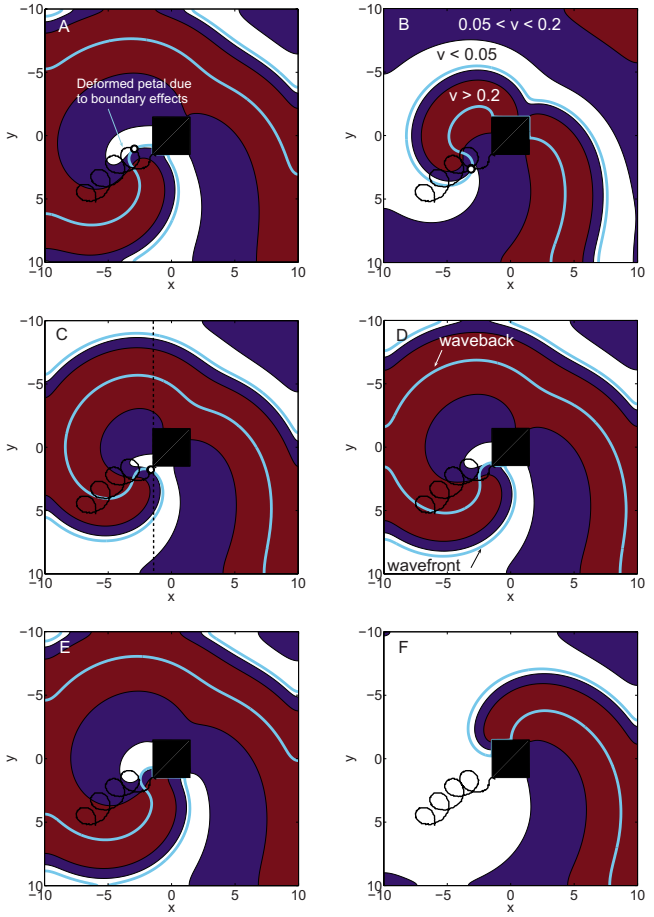

FIG. 5. (Color online) Interaction between a spiral wave obtained with the FHN equations and an obstacle for $t=89.2$, 91.6, 92.8, 93.2, 93.6, and 97.2 units of time from (A) to (F), respectively. The thick curves labeled as wavefront and waveback in frame (D) are given by the level curve $u=0.1$. The different colored regions represent different levels of refractoriness in the medium and are labeled in (B). The region $v \in [0,0.05]$, represents the completely and almost completely recovered medium; $v \in (0.05,0.2]$, is the region with partially recovered medium; $v>0.2$, is the region with the medium in completely refractory stage. The black dot filled in white is the location of the tip of the spiral wave at the specific time. In (A), the closest petal to the obstacle it was deformed due to a gain in curvature due to boundary effects [16]; [(B)–(D)] the tip of the spiral wave is very close to the obstacle; in (C) the vertical dashed line represents an imaginary boundary; (E) the tip of the spiral hits the obstacle; (F) the spiral wave is attached to the obstacle. (See text for details.) The initial condition is given by Eq. (2), with $x_0=-5$, $r_1=9.8$, $r_2=9$, $\alpha=-0.5$, and $t_s=2.5$.

the x and y directions, the obstacle started at the end of the subdomain $N_i=17$ and ended at the beginning of the subinterval $N_i=24$, i.e., the obstacle is given by the square $\Omega_1=\{(x,y)/-1.46\leq x\leq 1.46,-1.46\leq y\leq 1.46\}$. In order to get a spiral interacting with the obstacle, we initially carried out simulations in the R_∞ regime with no obstacles. After that, obstacles were placed in a position such that the interaction happened.

In [16], it was shown that spiral waves generated with the FHN model were reflected from the boundary independently of the incident angle θ_i. However, a different scenario is

obtained when the spiral interacts with a square obstacle as shown in Fig. 5. In the Figure, the interaction of the spiral wave with the obstacle for six different integration times is shown. The black square is the obstacle and the black dot filled in white gives the location of the tip; the bold line represents the level curve $u=0.1$, which gives the location of the wave front and the wave back of the spiral wave [labels on Fig. 5(D)]; the different colored regions represent different levels of refractoriness of the medium given by the v variable; the region $v \leq 0.05$ [Fig. 5(B)] means that the medium is recovered or almost recovered and an AP can be propagated easily; the region $v \in (0.05, 0.2)$ [Fig. 5(B)], implies that the medium is in refractory state but almost ready to be recovered. Propagation in this region is difficult. Finally, when $v \geq 0.2$ [Fig. 5(B)], the medium is not recovered at all and propagation in this region cannot occur.

From Figs. 5(A)–5(C), it is observed that the tip of the spiral gets really close to the obstacle. In Fig. 5(D), the tip of the spiral hits the obstacle, and finally in Fig. 5(E), the spiral wave attaches to the obstacle. The attachment of the spiral wave appears not to be consistent with [16], where for FHN, reflection of the spiral at a boundary was the only behavior obtained. In Fig. 5, we provide an explanation to clarify the situation. Figure 5(C) shows a vertical dashed line tangent to the left face of the obstacle. This line represents an imaginary boundary and can be thought that the spiral wave will hit this imaginary boundary. If we would have a boundary where the imaginary boundary is traced, then reflection of the spiral wave occurs.

The process of attachment of the spiral to the obstacle is as follows. Initially, we can think of the spiral wave moving toward the left face of the obstacle. In Fig. 5, it is shown that the unit of trajectory [16] closer to the obstacle is a distorted version of the units of trajectories that are far from the obstacle and the boundary domain. A unit of trajectory is the trajectory traced by the tip of the spiral in one rotation and consists of an arc and a petal. The change in shape is due to a gain in curvature of the tip trajectory due to the presence of a boundary (left side of the obstacle) as described in [17] and shown in Fig. 5(A). In Fig. 5(B), the tip of the spiral wave is located at an arc which means the medium is not completely recovered, so the tip traces a low curvature trajectory. In Fig. 5(C), the tip of the spiral gets close to the obstacle and moreover, part of the spiral wave has crossed the dotted line. In this case, the obstacle does not have any boundary effect on the tip trajectory and the spiral wave moves as if there is no boundary present. The wave propagates freely in the direction of the obstacle, and the medium ahead of the wave front next to the tip recovers completely facilitating the propagation of the spiral wave [Fig. 5(C)]. From the same figure, it is evident that the tip of the spiral wave is ready to trace another petal since the medium ahead of the front close to the tip is completely recovered. However, just before tracing a petal, the tip of the spiral wave encounters a corner of the obstacle [Fig. 5(D)]; in this case, the spiral wave does not have boundary effects near the tip as all these effects should have come from the imaginary boundary shown in Fig. 5(C). Finally, in Figs. 5(E) and 5(F), attachment to the obstacle is obtained.

It is important to note that attachment to the obstacle was possible due to the shape of the obstacle at the site of interaction, which was a corner. From this, it follows that one of the conditions to observe attachment is the shape of the obstacle at the site of collision. From Fig. 5, it is clear that because the spiral wave has hit the obstacle at a corner, attachment was observed. If the obstacle is large and the interaction of the spiral wave hits the obstacle at a face, then reflection would have occurred. A second condition needed to observe attachment is the size of the obstacle. A very small obstacle will imply that attachment is not possible as the spiral tip would complete a cycle around the obstacle in a time shorter than the refractory period of the tissue. Therefore, a minimum size of the obstacle is needed [29]. Two more properties that will give conditions for attachment to the obstacle will be discussed in detail in the next section in connection with the MFHN equations.

C. Interaction of spirals with obstacles for the MFHN model

For this model, it follows from the results in Sec. IV A that attachment of a spiral wave to an obstacle without corners is expected to occur. We now focus on the interaction of the region near the tip of a spiral wave generated with the MFHN equations ($\delta_1=0.6$) and an obstacle. In particular, we consider that such interaction takes place at the lower face of the obstacle as shown in Fig. 6. The angle of incidence is $\theta_i=52.8°$, for which reflection of the spiral wave is expected as shown in Fig. 4 if the interaction takes place at a boundary.

In Fig. 6, we summarize the results obtained from the interaction between the spiral wave and two different obstacles. In the figure, it is shown the interaction with the first and second obstacle in the left [Figs. 6(A)–6(C)] and right [Figs. 6(D) and 6(E)] columns, respectively. In the simulations, we fixed the size and position of the obstacle in the y direction with the same values as in the previous subsection. However, in the x direction, we varied the size of the obstacle by fixing the right position of the obstacle at the beginning of the subinterval $N_i=26$ and varying the left position where the obstacle begins. In the left and right columns of Fig. 6, the obstacle starts at the end of the subinterval $N_i=15$ and 16, respectively. Therefore, the obstacles are given by the squares $\Omega_1=\{(x,y)/-2.46\leq x\leq 2.46, -1.46\leq y\leq 1.46\}$ and $\Omega_2=\{(x,y)/-1.96\leq x\leq 2.46, -1.46\leq y\leq 1.46\}$ for the left and right columns in Fig. 6, respectively.

For each of the two obstacles considered, a spiral wave was generated in such a way that the tip traces the same trajectory until it hits the obstacle. It is important to mention that for each of the results found for the obstacles that started at the beginning of the subintervals $N_i=15$ and 16, different runs were taken with different values at which the obstacle ended in the y direction ($N_i>24$). The phenomena observed were the same, as for those where the obstacle ended at the beginning of the subinterval $N_i=24$. With this procedure, we remove the dependence of the length of the lower face and focus only on the location of the site of interaction.

In Fig. 6, the solutions for the two different obstacles are shown for three different integration times, such that the frame pairs (A,D), (B,E), and (C,F) are shown for exactly the

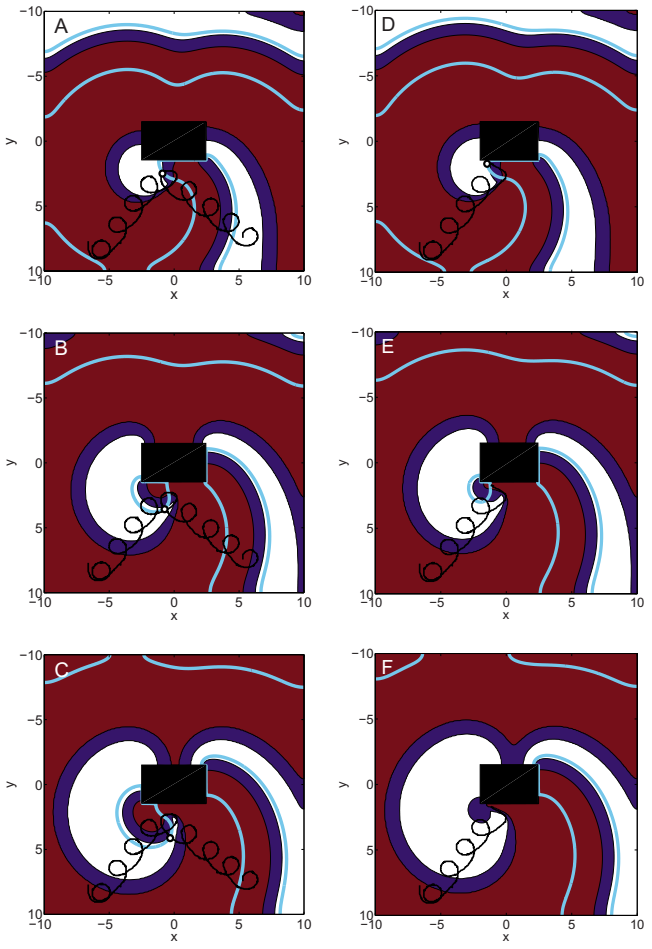

FIG. 6. (Color online) Interaction between a spiral wave obtained with the MFHN equations and obstacles for $t_1=40.25$, $t_2=40.95$, and $t_3=41.3$ units of time. [(A)–(C)] The obstacle in the x direction starts at the end of the subinterval $N_i=15$ and ends at the beginning of the subinterval $N_i=26$; [(D)–(F)] the obstacle in the x direction starts at the end of the subinterval $N_i=16$ and ends at the beginning of the subinterval $N_i=26$. Plot pairs (A,D), (B,E), and (C,F) correspond to $t=t_1$, t_2, and $t=t_3$, respectively. (See text for explanation.) The initial condition is given by Eq. (2), with $x_0=-6$, $r_1=11$, $r_2=9$, $\alpha=-0.262$, and $t_s=1.4$. The obstacle was placed at time $t^*=26$.

same integration times. In this way, it is possible to observe the qualitative differences in the dynamics at a fixed time. In Figs. 6(A)–6(C) it is observed that the spiral wave gets reflected whereas for the case of the shortened obstacle, shown in Figs. 6(D)–6(F), attachment of the spiral wave to the obstacle is observed. In Fig. 6(A), the part of the spiral close to the tip of the spiral wave gets close to the lower face of the obstacle. Due to boundary effects, the tip trajectory gains more curvature as the area to be excited is less compared to the case when no obstacle is present. A similar situation occurs for the case of the shortened obstacle [Fig. 6(D)], i.e., the tip trajectory changes direction due to the presence of the obstacle. The effect of gaining curvature due to the presence of a boundary is discussed in [16,17].

The important point is that for Fig. 6(D), the interaction is closer to the left bottom corner than the case in Fig. 6(A).

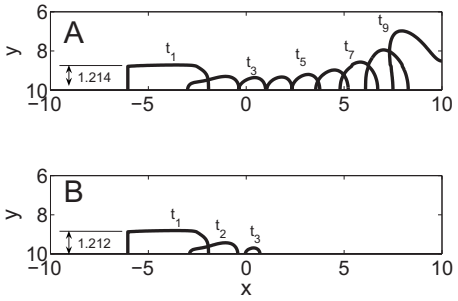

FIG. 7. Propagating front with a free end generated with the FHN equations. (A) When the length of the propagating front is above a critical value, the free end propagates in the medium and a spiral is formed. This case corresponds to reflection; (B) the length of the propagating front is below the critical value, and the free end dies out. This corresponds to the case of attachment.

Therefore, the front in Fig. 6(D) arrives at the corner earlier than the front in Fig. 6(A). At that point, the area to be excited by the front in Fig. 6(D) is larger than the area that the front in Fig. 6(A) has to excite. As a result, the front in Fig. 6(A) is able to propagate and Fig. 6(B) is obtained. Finally, in Fig. 6(C), the front continues propagating and reflection is observed. From Fig. 6(D), the area that needs to be excited has become too large compared to the length of the front of the spiral close to the tip. Therefore, propagation fails as the front dies out as shown in consecutive frames in Figs. 6(E) and 6(F). As shown in Fig. 6(F), attachment has been obtained.

The argument considered in this section to demonstrate attachment is based on the fact that the front near the tip it is incapable of propagating because the area that has to be excited becomes too large for the front. To understand better this argument, we focus on the propagation of a free end (Fig. 7). In the figure, we considered a simulation of the FHN equations [Eq. (1), with $\delta=1$] with parameters $a=0.52$, $b=0.05$, and $\epsilon=0.02$. With these parameters, the tip of the spiral wave traces a circular trajectory. Therefore, an initial pulse was originated on the domain $[-10,10]\times[-10,10]$ with the initial condition given by

$$u(x,y)=\{1+\exp[4(|x|-9.8)]\}^{-2}-\{1+\exp[4(|x|-9)]\}^{-2}, \tag{3}$$

where u was redefined as zero for $x>0$. Therefore, the pulse travels from left to right inside the domain, and then, for the time interval $t=[2.1,2.2]$, the front is redefined as $u=0$ and $v=0.25$ for $y<y_0$ giving a propagating free end. In Fig. 7, the value of y_0 was taken as 8.786 and 8.788 for Figs. 7(A) and 7(B), respectively. With this procedure, two different free ends with initial front length of 1.214 and 1.212 units of distance are generated and shown in Figs. 7(A) and 7(B), respectively. In Fig. 7(A), are shown nine snapshots of the level curve $u=0.27$ for different integration times. The figure shows that the length of the front (which initially was 1.214) gets reduced and for the times t_2 to t_4, the length of this front is maintained. The free end shown in t_5 starts growing until t_9, where it follows that the free end will evolve into a spiral wave.

The results when the value of y_0 is changed to 8.788 are shown in Fig. 7(B). In this case, the length of the initial front is 1.212 units of distance. In Fig. 7(B), level curves of $u=0.27$ for three different integration times are shown. By contrast to the previous case, it is shown that the initial free end shrinks and disappears from the domain.

It follows from Fig. 7 that if we have a pulse with a free end propagating in a medium with a fixed excitability ahead of this propagating pulse, then, there is a relationship between the length of the wave front and the fixed area to be excited. When the length of the front of this pulse has a critical length l^*, then, below this critical length the pulse will disappear and above this value the free end will remain inside the domain and generate a spiral wave. This property has been considered previously indirectly in computational and experimental studies where a pulse has to excite an area after it has passed across an isthmus [30,31].

Based on the studies presented in this section, and the argument from Fig. 7, it is clear that attachment of a spiral wave to an obstacle depends on the length of the front near the tip of the spiral wave and the area to be excited by this front. This argument for attachment is the third property that should be considered in order to obtain attachment of a spiral wave to an obstacle.

The last property of the four mentioned in this work is related to the third property just discussed. This property is the excitability of the medium where the front has to propagate. Clearly, if we have a fixed length of the front and a fixed area to be excited, we also have to take into account the degree of excitability of the area to be excited or the strength of the pulse to propagate. This last property is explained in [32,33] with a study of propagating pulses with a free end. If the excitability of the medium is high, then the propagating pulse will evolve into a spiral wave, whereas if it is low, then the pulse will shrink and disappear. The excitability of the medium is responsible for giving the different trajectories of the tip of the spiral wave, particularly, the R_∞ regime studied here. It is also responsible for the reflection and annihilation of a spiral wave at a boundary as seen in [16].

D. BR model

In this section, we consider the interaction of a spiral wave in the meandering regime generated with the BR model [26] and an obstacle. The objective is to show that the properties obtained for the MFHN equations are sufficiently realistic so as to model attachment to an obstacle. We used the BR model with the parameters $g_{Na}=2.37$, $g_{NaC}=0.003$, $E_{Na}=50.0$, and $g_S=0.03$ as in [16] to generate spiral waves in the R_∞ regime. In the simulations, each dimension was discretized with $N_i=180$ subintervals and $N_c=5$ points in each subinterval as in [16]. Two different obstacle sizes were considered (right and left columns in Fig. 8). In both cases, in the y direction, the obstacles start at the end of the subinterval $N_i=20$ and end at the beginning of the subinterval $N_i=40$. In the x direction, the obstacles end at the beginning of the subinterval $N_i=130$ and start at the end of the subintervals $N_i=80$ and $N_i=84$, respectively. Therefore, the obstacles are given by the squares

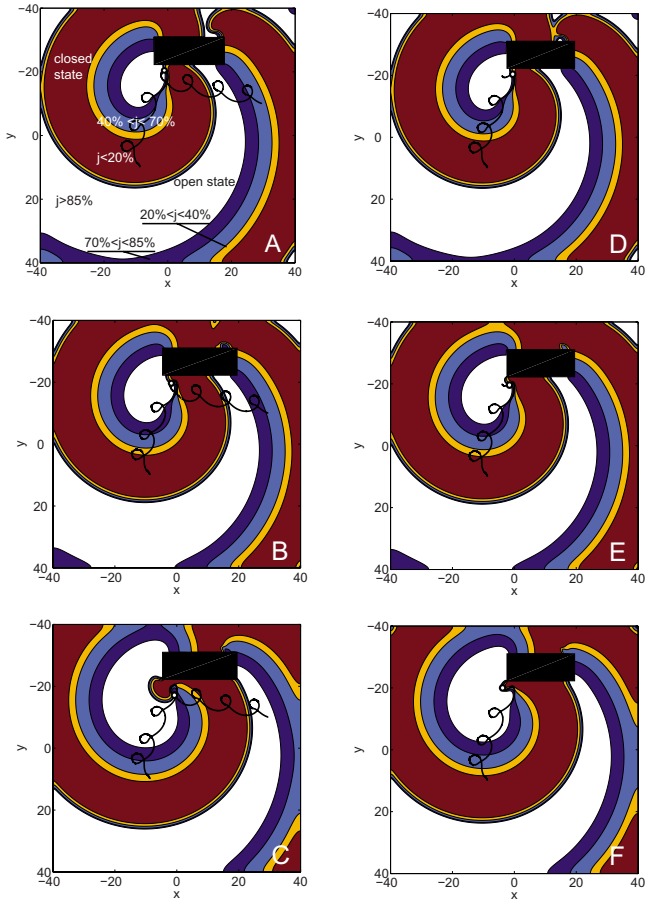

FIG. 8. (Color online) Interaction of a spiral wave generated with the BR model and two different cases of obstacles for $t_1=591.92$, $t_2=599.4$, and $t_3=614.36$ ms. In (A)–(C) reflection is observed and; (D)–(F) attachment is observed. Plot pairs (A,D), (B,E), and (C,F) correspond to $t=t_1$, t_2, and $t=t_3$, respectively. (See text for details.)

$\Omega_1=\{(x,y)/-0.95\leq x\leq 4.12,-7.52\leq y\leq -5.73\}$ and $\Omega_2=\{(x,y)/-0.51\leq x\leq 4.12-7.52\leq y\leq -5.73\}$ for the left and right columns in Fig. 8, respectively. In Fig. 8, we plot contour plots of the variable j, which is responsible for the reactivation of the medium, as done in [16]. When $j<20\%$, means that the sodium gate is still closed and no action potential can be elicited here. When $j>85\%$ means that the medium is ready or almost ready to accept an action potential. The rest of the states, $20\%<j<40\%$, $40\%<j<70\%$, and $70\%<j<85\%$ are intermediate stages of the j variable.

A spiral wave was generated as done in [16] with $\alpha=0$, $c_1=40$, $c_2=39$, $y_0=-10$, and $t_g=150$ ms. The obstacle was inserted at $t=t_g$ ms. The interaction between the spiral wave and the obstacles Ω_1 and Ω_2 is shown in Figs. 8(A)–8(F), respectively, for three integration times. In Figs. 8(A)–8(C) reflection of the spiral wave at the obstacle is observed, whereas in Figs. 8(D)–8(F), attachment occurs.

From Fig. 8(A), the front of the spiral wave close to the tip hits the boundary on the lower face. The short length wave-front is able to excite the area ahead of it [Figs. 8(B) and 8(C)]. It follows that the front propagates generating a spiral wave, giving as a result reflection of the spiral at the obstacle [Fig. 8(C)]. A different scenario occurs when the

length of the obstacle in the positive x direction is decreased, as shown in Figs. 8(D)–8(F). Here, the interaction of the spiral wave takes place closer to the corner than in the previous case [Figs. 8(A)–8(C)]. The same short length wavefront has to excite now a larger area, as a consequence of being closer to the corner of the obstacle. The propagating front is not able to excite this larger area and dies out giving attachment of the spiral wave to the obstacle [Fig. 8(F)].

V. SUMMARY AND DISCUSSION

Numerical studies of spiral waves obtained with FHN, MFHN, and BR equations were considered in the present paper. In [16], it was shown that a spiral wave in the R_∞ regime generated with the FHN dynamics does not annihilate at the boundary. This was due to the fact that the value of η defined in Sec. IV A was too small and it was not possible to get an interaction of the trajectory of the tip and the boundary when the tip was located at an arc. However, with the MFHN equations, it was possible to increase the value of η such that the probability of hitting the boundary with an arc was also increased. Therefore, it was possible to obtain annihilation of the spiral wave at the boundary, just as shown with the BR equations [16].

The interaction between spiral waves and rectangular obstacles [Secs. IV B and IV C] was also studied in this work. The case of annihilation of a spiral wave at the boundary was not observed for the FHN equations. However, when the boundary was changed to an obstacle [Sec. IV B] attachment of the spiral to the obstacle was observed. This was because the spiral wave hits the obstacle at a corner.

When spiral waves generated with the MFHN equations [Sec. IV C] were considered, the attachment to the obstacle was anticipated as based on Fig. 4. The length of the lower face of the obstacle was varied taking a spiral wave that had an incident angle such that reflection at a domain boundary is observed and therefore giving an interaction of the spiral wave at places far and close to one of the corners of the obstacle. In this experiment, both reflection and attachment were observed. The attachment occurred because the area to be excited by the front of the spiral wave close to the tip was too large, and the front died giving attachment to the obstacle.

It was shown that the same attachment situation observed for MFHN equations occurred for the BR model [Sec. IV D]. Therefore, the attachment properties remain valid for spiral waves based on a physiological model. In the physiological model it is possible to find which values of the realistic parameters are responsible for the meandering regime. Based on this information, it is possible to determine the size and geometry of the obstacle in such way that it maximizes the possibility of attachment. However, this issue is out of the scope of the study presented here.

In the present study, linear trajectories which arise more commonly in experiments ([1] and references therein) were not considered. Linear trajectories can be seen as a limiting case where the size of a petal has gone to zero or to a very small value, and the length of an arc has reached some finite value. In this case η tends to infinity or to a very large value. In this case, attachment is expected.

Four properties for attachment were considered in this work: the size of the obstacle, the geometry of the obstacle at the site of interaction, the excitability of the medium where the front has to propagate, and the ratio of the area to be excited and the length of the front close to the tip trajectory responsible of keeping the spiral inside the domain. Therefore, this work extends the idea of the attachment of a spiral wave to an obstacle. In [10], it was experimentally shown that a spiral wave always attaches to an obstacle of some minimum size. However, according to the results presented in this work, the size of the obstacle is not the only property necessary to obtain attachment.

One of the main limitations of the numerical method considered in this work is the restriction of the shape and size of the obstacles to rectangular geometries, which depend on N_i and N_{ch}. In the simulations, the dimensions of the obstacle increased or decreased in multiples of N_{ch}. This limitation did not allow us to study more precisely the transition between reflection and annihilation of the spiral wave at the obstacle.

Another limitation in this paper was the restriction to the R_∞ case. Interaction between meandering spiral waves with trajectories tracing epitrochoids or hypotrochoids and obstacles are more complex to analyze. Even that it is possible to approximate such interaction with the R_∞ case, it is not possible to provide a long time behavior of the dynamics due to the possible repetitive interactions that are not observed with the R_∞ case.

Future studies will consider the simulation of the interaction between spiral waves and obstacles with more general shapes and in more general regimes of a spiral wave, such as the case of epitrochoids and hypotrocoids.

ACKNOWLEDGMENTS

The author is grateful to the referees for their valuable comments and suggestions. The author is also grateful to Flavio H. Fenton and Alexander V. Panfilov for very useful discussions. Special thanks to Bernie Shizgal for reading the paper prior to publication. The author would like to acknowledge ACARUS at the University of Sonora, for their facilities for the numerical computations. This work was supported by CONACYT.

[1] F. H. Fenton, E. Cherry, H. M. Hastings, and S. J. Evans, Chaos **12**, 852 (2002).
[2] M. A. Dahlem and S. C. Müller, Exp. Brain Res. **115**, 319 (1997).
[3] J. P. Keener and J. Sneyd, *Mathematical Physiology: Interdisciplinary Applied Mathematics* (Springer, New York, 1998).
[4] J. Tyson, Lect. Notes Biomath. **100**, 569 (1994).
[5] A. T. Winfree, Chaos **8**, 1 (1998).

[6] A. V. Panfilov and J. P. Keener, Chaos, Solitons Fractals **5**, 681 (1995).
[7] J. J. Tyson and J. P. Keener, Physica D **32**, 327 (1988).
[8] A. T. Winfree, Chaos **1**, 303 (1991).
[9] E. M. Azene, N. A. Trayanova, and E. Warman, Ann. Biomed. Eng. **29**, 35 (2001).
[10] T. Ikeda, M. Yashima, T. Uchida, D. Hough, M. C. Fishbein, W. J. Mandel, P.-S. Chen, and H. S. Karagueuzian, Circ. Res. **81**, 753 (1997).
[11] A. V. Panfilov and J. P. Keener, J. Theor. Biol. **163**, 439 (1993).
[12] T. K. Shajahan, S. Sinha, and R. Pandit, Phys. Rev. E **75**, 011929 (2007).
[13] P. Comtois and A. Vinet, Phys. Rev. E **72**, 051927 (2005).
[14] Z. Y. Lim, B. Maskara, F. Aguel, R. Emokpae, and L. Tung, Circulation **114**, 2113 (2006).
[15] Y.-H. Kim, F. Xie, M. Yashima, T.-J. Wu, M. Valderrábano, M.-H. Lee, T. Ohara, O. Voroshilovsky, R. N. Doshi, M. C. Fishbein, Z. Qu, A. Garfinkel, J. N. Weiss, H. S. Karagueuzian, and P.-S. Chen, Circulation **100**, 1450 (1999).
[16] D. Olmos and B. D. Shizgal, Phys. Rev. E **77**, 031918 (2008).
[17] Ye. A. Yermakova and A. M. Pertsov, Biophysics (Engl. Transl.) **31**, 932 (1986).
[18] O. Bernus, R. Wilders, C. W. Zemlin, H. Verschelde, and A. V. Panfilov, Am. J. Physiol. Heart Circ. Physiol. **282**, H2296 (2002).
[19] L. Priebe and D. J. Beuckelmann, Circ. Res. **82**, 1206 (1998).
[20] K. H. W. J. Ten Tusscher and A. V. Panfilov, Phys. Med. Biol. **51**, 6141 (2006).
[21] K. H. W. J. ten Tusscher and A. V. Panfilov, Am. J. Physiol. Heart Circ. Physiol. **291**, H1088 (2006).
[22] A. V. Panfilov and J. P. Keener, J. Cardiovasc. Electrophysiol. **4**, 412 (1993).
[23] A. Bueno-Orovio, E. M. Cherry, and F. H. Fenton, J. Theor. Biol. **253**, 544 (2008).
[24] D. Barkley, Physica D **49**, 61 (1991).
[25] A. V. Panfilov, Chaos **8**, 57 (1998).
[26] G. W. Beeler and H. Reuter, J. Physiol. (London) **268**, 177 (1977).
[27] D. Olmos and B. D. Shizgal, Math. Comput. Simul. **79**, 2258 (2009).
[28] A. Bueno-Orovio, V. M. Pérez-García, and F. H. Fenton, J. Sci. Comput. **28**, 886 (2006).
[29] M. A. Allessie, F. I. Bonke, and F. J. Schopman, Circ. Res. **41**, 9 (1977).
[30] D. de la Fuente, B. Sasyniuk, and G. K. Moe, Circulation **44**, 803 (1971).
[31] C. Cabo, A. M. Pertsov, W. T. Baxter, J. M. Davidenko, R. A. Gray, and J. Jalife, Circ. Res. **75**, 1014 (1994).
[32] A. S. Mikhailov, V. A. Davydov, and V. S. Zykov, Physica D **70**, 1 (1994).
[33] I. R. Efimov, V. I. Krinsky, and J. Jalife, Chaos, Solitons Fractals **5**, 513 (1995).